New patterns of centrifugally driven thermal convection

M. Jaletzky and F. H. Busse*

Institute of Physics, University of Bayreuth D-95440 Bayreuth, Germany

Contributed by Friedrich Busse, December 20, 1999

An experimental study is described of convection driven by thermal buoyancy in the annular gap between two corotating coaxial cylinders, heated from the outside and cooled from the inside. Steady convection patterns of the hexaroll and of the knot type are observed in the case of high Prandtl number fluids, for which the Coriolis force is sufficiently small. Oblique rolls and phase turbulence in the form of irregular patterns of convection can also be observed in wide regions of the parameter space.

1. Introduction

Rayleigh–Bénard convection in a horizontal layer heated from below has become the favored example for the study of the spontaneous formation of structures in hydrodynamic systems. Because the physical conditions are not only homogeneous, but also isotropic in the horizontal directions if the aspect ratio of the layer is sufficiently large, different patterns of convection can compete in the neighborhood of the critical parameters for the onset of convective instability. Owing to small deviations from the Boussinesq approximation the temperature dependence of material properties is not entirely negligible in experimental realizations and therefore hexagonal cells are usually observed at onset. They are replaced by rolls as the temperature contrast is increased unless the properties of the fluid layer are strongly asymmetric with respect to its midplane. Square like convection cells can be found when upper and lower boundaries do not conduct heat very well. For these and other properties of thermal convection we refer to the review of Busse (1).

In this paper, we describe an experiment where gravity as the origin of buoyancy is replaced by the centrifugal force. The Rayleigh–Bénard layer is wrapped around a vertical cylinder—so to speak—and the system is rotating sufficiently rapidly such that the centrifugal force exceeds gravity by a large margin. There is also the Coriolis force, of course, which causes differences with respect to the ordinary Rayleigh–Bénard layer. In fact the Coriolis force is typically a dominating force ensuring that convection assumes the form of rolls aligned parallel to the axis of rotation (2). But for fluids of sufficiently large Prandtl number a limit can be reached in which the Coriolis force can be regarded as a small perturbation in the balance of forces in Rayleigh–Bénard convection. The experimental study of this paper focuses on this limit.

From the theoretical point of view this limit is of interest since it represents the influence of a special small anisotropy on an isotropic system. The isotropy in the axial and azimuthal directions is attained in the small gap limit of the system. A theoretical investigation of the problem by Auer *et al.* (3) has revealed some interesting new patterns evolving from instabilities of the axially aligned convection rolls. These findings have provided the motivation for the experimental study. But the mathematical analysis of the nonlinear properties of convection has been incomplete. Besides the predicted forms of convection other types of patterns such as oblique rolls have also been observed in the experiment. The mathematical analysis of these patterns and of the associated phenomenon of phase turbulence is the topic of ongoing research, a preliminary report of which has been included in the review of Busse *et al.* (4).

In the following section, the experimental setup is described and its main parameters are introduced. Section 3 is devoted to the steady patterns of convection observed in the experiment, and Section 4 describes spatio-temporally chaotic convection flows. In a concluding section, some not yet fully understood properties of the system are discussed in relationship to the theoretical results.

2. Experimental Apparatus and Methods

A sketch of the rotating cylindrical annulus apparatus is given in Fig. 1. For the purpose of visualization, an outer glass cylinder made from a calibrated precision glass tube (Schott GmbH) with a inner radius of 70 mm is used. Two different inner cylinders made of aluminium are used with outer radii of 64.85 mm and 66.95 mm, respectively, such that the fluid layers with thicknesses $d = 5.15$ mm and $d = 3.05$ mm can be realized. These values are averages over the circumference of the cylindrical surfaces. Variations of the order of a few tenths of 1 mm must be expected. The axial height of the fluid filled gap is 163 mm. The cylindrical manifold is rotated at rates of up to 900 rpm in a plexiglas box through which thermostatically controlled water is circulated. While the outer cylinder is thus readily kept at constant temperature, the cooling of the inner cylinder is more difficult. Cold water from a second thermostat is circulated through the rotating hollow shaft into the inner cylinder with the help of a stationary tube inserted along the axis of the hollow shaft. Baffles are fixed at the end of the hollow shaft near the bottom of the inner cylinder, such that the cooling water is distributed to the cylindrical wall as shown in Fig. 1.

For the purpose of visualization, plastic sheets with embedded thermochromatic liquid crystals (supplied by Hallcrest Inc., U.K.) are glued to the outer wall of the inner cylinder. Sometimes these sheets have also been fixed to the inner side of the outer glass cylinder. The temperatures of the cylinders can be kept constant within a few hundredths of 1°C, and the mean temperature is chosen such that the best contrast is obtained of the color play induced by convection in the thermochromatic liquid crystal sheet. In the case of time-dependent convection, the temperature fluctuations can be measured by thermistors embedded in the outer wall of the inner cylinder at its equator. Particular attention has been paid to the constancy of the rotation rate. Through the use of an electronically controlled motor (motor-tachogenerator combination of Mattke GmbH, Freiburg, Germany), the relative variations of the angular velocity of the cylindrical manifold could be kept well below 10^{-4}. Pictures are taken photographically or with a charge-coupled device camera. For this purpose the apparatus is illuminated with a triggered flash.

Although the characteristic thermal time scale, d^2/κ, of the fluid layer, where κ is the thermal diffusivity, is only a few min-

*To whom reprint requests should be addressed. E-mail Busse@uni-bayreuth.de.

The publication costs of this article were defrayed in part by page charge payment. This article must therefore be hereby marked "*advertisement*" in accordance with 18 U.S.C. §1734 soley to indicate this fact.

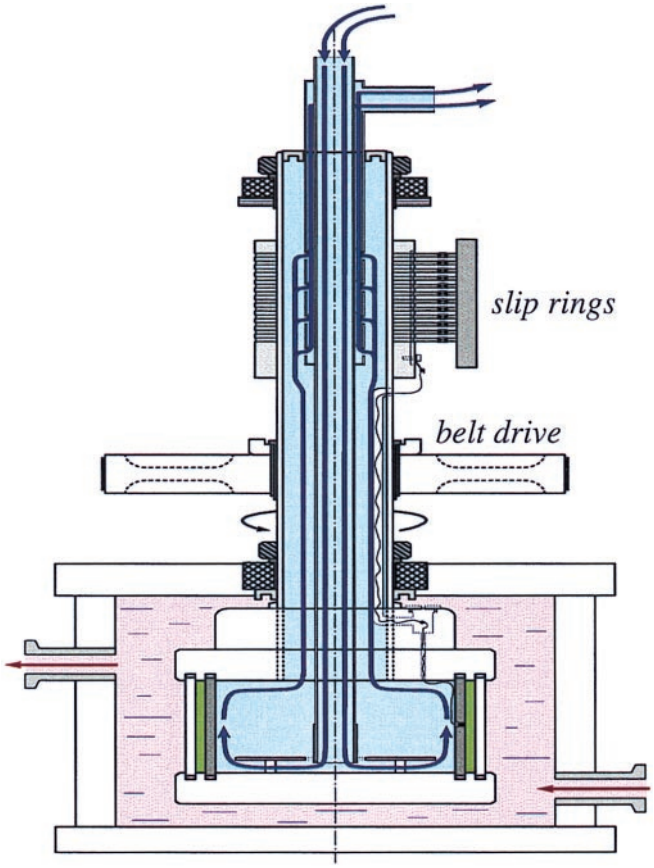

Fig. 1. Sketch of the experimental apparatus. Red (blue) indicates circulating warm (cold) water. The convecting fluid is shown in green.

utes at most, it is usually necessary to wait for about an hour before a thermally stationary state can be expected. To change the parameters of the system it is easier to change the rotation rate. But this procedure has the disadvantage that the Rayleigh number R and the Coriolis parameter τ are changed at the same time. These parameters and the Prandtl number are defined by

$$R = \frac{\gamma(T_2 - T_1)\Omega^2 r_m d^3}{\nu\kappa}, \quad \tau = \frac{\Omega d^2}{\nu}, \quad P = \frac{\nu}{\kappa} \qquad [1]$$

where T_1 and T_2 are the temperatures of the inner and outer cylindrical walls of the annular fluid layer, r_m is its mean radius, and γ and ν are the thermal expansivity and the kinematic viscosity of the fluid. Ω is the angular velocity of rotation. Since the Rayleigh number R can be expressed in the form

$$R = \gamma(T_2 - T_1)\tau^2 r_m P/d, \qquad [2]$$

it is clear that the limit of vanishing τ can only be achieved in the limit of large Prandtl numbers if the quantity $\gamma(T_2 - T_1)$ denoting the relative change in density between walls is kept sufficiently small to satisfy the assumption of a Boussinesq fluid. Although the anisotropy present in the layer can be noticed for rather small values of τ, the Coriolis force has a negligible effect for $\tau \leqslant 1$. This is evident from the values R for the onset of convection in the form of rolls inclined with the angle χ with respect to the axis of rotation (3)

$$R = 1707.8 + \tau^2 4\sin^2\chi. \qquad [3]$$

A 1% change in the Rayleigh number for the onset of axisymmetric rolls ($\chi = \pi/2$) which are most affected by the Coriolis force requires $\tau > 2$.

Table 1. Properties of liquids (properties of silicone oils as provided by the manufacturer, Bayer AG)

Liquid	Silicone oils			Glycerol
	M200	M350	M500	at 34.7°C
$\nu[10^{-6}m^2/s]$	200	350	500	370
$\gamma[10^{-5}K^{-1}]$	99	99	99	50
$\varrho[kg/m^3]$	970	970	970	1252
$c_p[J/gK]$	1.51	1.51	1.51	2.39
$\lambda[W/mK]$	0.165	0.167	0.174	0.285

Two types of high Prandtl number fluids have been used. Glycerol and glycerol-water mixtures cover a wide range of viscosities and offer the advantage that thermochromatic liquid crystals can be suspended which initially was the preferred method of visualization. Most later experiments have been done with silicone oils which tend to dissolve the coated liquid crystals, but do not affect the liquid crystals embedded in plastic sheets and offer the advantage that their properties do not depend much on temperature. Typical properties of examples of the two kinds of liquids are given in Table 1.

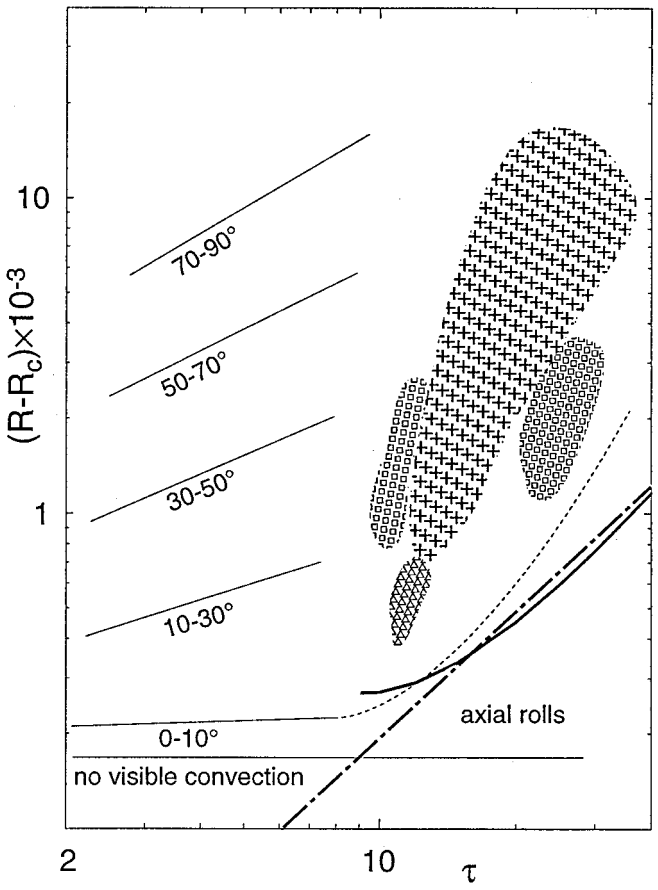

Fig. 2. Regions in the R-τ-plane where different patterns of convection have been observed. Axial and oblique rolls are observed in the region where the angles of inclination have been indicated. Regions indicated by triangles and squares refer to hexarolls and knot convection, respectively. Crosses indicate phase turbulent convection. In the blanc areas between different patterns usually mixtures of these patterns have been observed. In the region close to the ordinate hexagons have been observed. The dash-dotted line indicates the onset of the hexaroll instabilities and the thick solid line denotes the onset of the knot instability according to ref. 3.

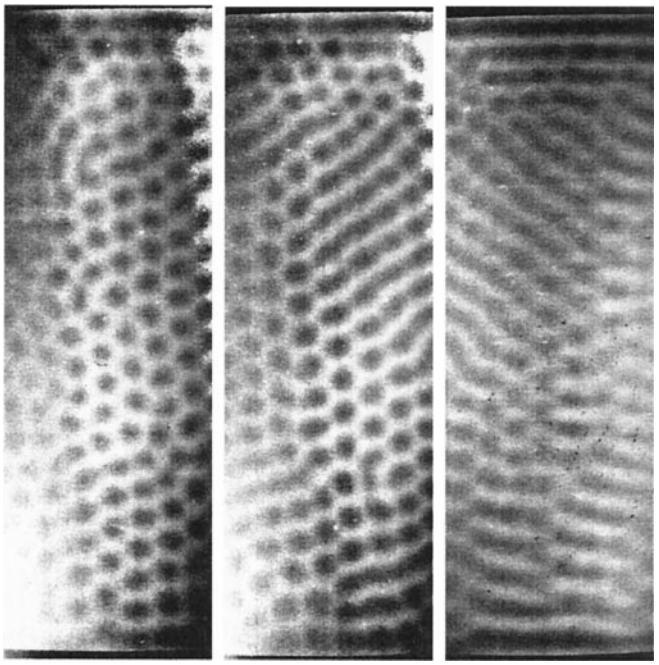

Fig. 3. Hexagonal convection and transition to oblique rolls observed in glycerol with a mean temperature of 34.7°C. The computer-enhanced photographs correspond to the parameter values $R = 2670, 3130, 3375$, $\tau = 1.8, 2.0, 2.1$ (left to right).

3. Steady Patterns of Convection

A general overview of the various states of convection can be gathered from Fig. 2. For sufficiently small values of τ the properties of an isotropic Rayleigh–Bénard layer are approximately recovered. Depending on the size of the deviations from the Boussinesq limit of the fluid properties, hexagonal convection cells are observed for a varying range of Rayleigh numbers R above the critical value $R_c \approx 1708$. The experiment carried out with glycerol exhibits a larger range for which hexagonal cells can be observed as shown in Fig. 3 than the experiments with silicone oils since the latter are characterized by a much smaller temperature dependence of the viscosity than glycerol or glycerol-water mixtures.

While the regime in which hexagonal convection cells are observed differs for silicone oils and for glycerol-water mixtures and for this reason has not been indicated in Fig. 2, the occurence of the other convection pattern appears to be not much influenced by the properties of the liquids. As soon as the transition from hexagonal convection to roll convection occurs (see, for instance, ref. 5) the influence of the Coriolis force becomes noticeable even in the limit of small τ in that the rolls are oriented with a specific angle with respect to the axis of rotation. Curiously, rolls aligned with the axis of rotation are not preferred for values of the supercritical value $R - R_c$ of the order of 10^3 or higher, as one might expect from relationship **3**. For $\tau \gtrsim 1$ the onset of convection occurs in the form of axially aligned rolls, but, unless τ is much larger than 10, these are replaced by oblique rolls as the Rayleigh number is increased as illustrated in Fig. 4. The angle of inclination with respect to the direction of the axis increases with increasing R as indicated in Fig. 2 until nearly axisymmetric rolls are observed at Rayleigh number of the order of 5 times the critical value.

An interesting novel kind of stationary convection is knot convection. The name "knot convection" originally introduced by Busse and Clever (6) for a three-dimensional steady convection flow realized in a planar Rayleigh–Bénard layer has been retained because the instability continuously evolves from limit

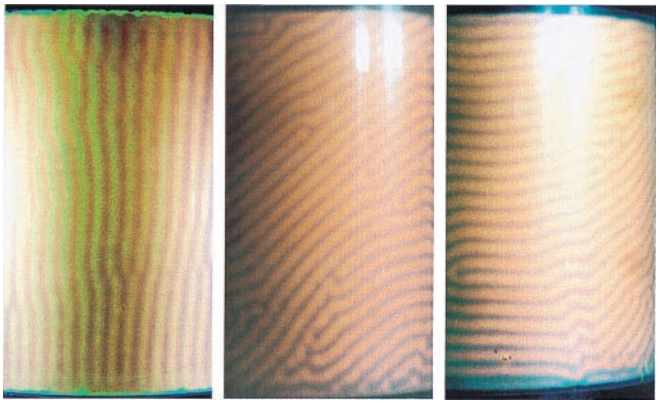

Fig. 4. Oblique rolls in silicone oil with increasing angle of inclination. The photographs correspond to the parameter values $R = 2320, 2880, 3630$, $\tau = 3.7, 4.1, 4.6$.

$\tau = 0$ as shown in the numerical computations of Auer *et al.* (3) for $P = 7$. The transition to knot convection can be observed for $\tau \gtrsim 5$ and the corresponding Rayleigh numbers are in reasonable agreement with the theoretical prediction. Some deviations between theory and experiment must be expected because the computed stability boundary shown in Fig. 2 has been obtained for axially aligned rolls while the transition to knot convection in the experiments occurs from slightly oblique rolls.

Because of the effects of rotation, the characteristic knots are no longer located symmetrically on the sheets of rising and descending fluid flow as in the case $\tau = 0$ but are shifted into an asymmetric position as shown in the experimental observation of Fig. 5. A theoretical computation of knot convection is shown in Fig. 6 and exhibits fair agreement with the realized pattern.

The hexaroll pattern of convection is rather similar to knot convection except for the characteristic difference in symmetry as shown in the experimental and theoretical examples of Figs. 5 and 6. The experimental parameters for observations of hexarolls show little relationship to the theoretically determined stability boundary of axially rolls (3). The reason for this discrepancy lies in the subcritical bifurcation of the steady hexaroll

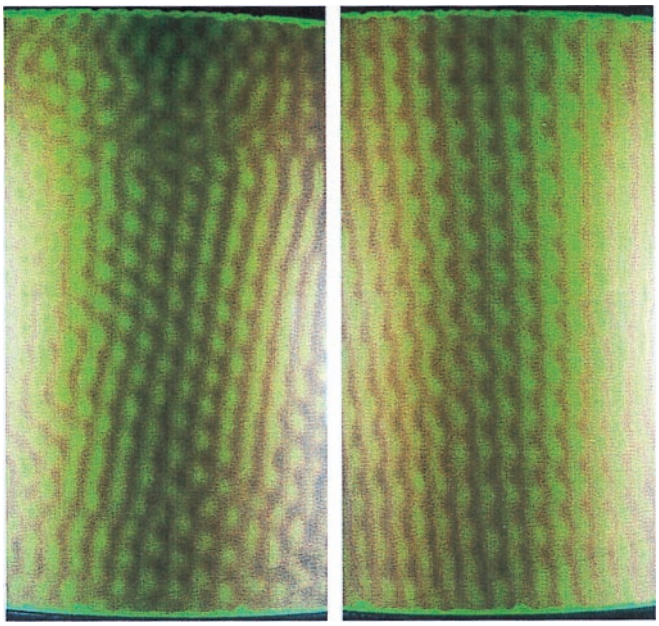

Fig. 5. Hexarolls (left) with $R = 2290$, $\tau = 10$ and knot convection (right) with $R = 4600$, $\tau = 24$ observed in silicone oil. Direction of rotation is toward the right.

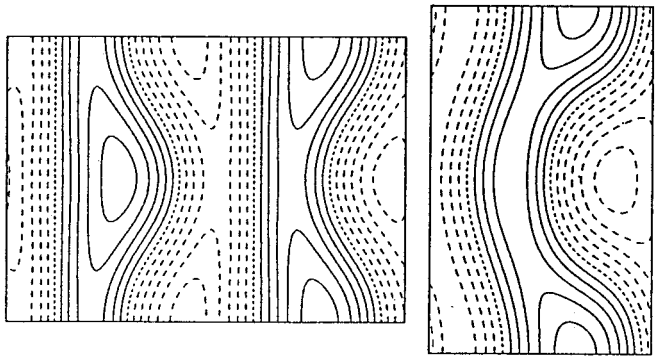

Fig. 6. Isotherms of hexarolls (*Left*) and knots (*Right*) in the midplane of the layer computed in the small gap approximation after Busse and Clever (7). The left (right) plot corresponds to $R = 2{,}300$ (2,400), $\alpha_x = 2.2$ (2.0) and $\alpha_y = 1.559$ (3.117), where α_x, α_y denote the wavenumbers in the axial and the azimuthal directions made dimensionless with the gap width d. The parameter values $P = 10^3$, $\tau = 20$ were used in both cases. Direction of rotation is toward the right.

solution. The theoretical analysis of the bifurcation structure is quite complex and will be addressed in a future publication (M. Zaks, private communication).

4. Time-Dependent Convection Flows

The subcritical nature of the bifurcation of the hexarolls from axial rolls leads to the phenomenon of phase turbulence. So far this phenomenon has been studied only theoretically (4,7) and attempts to identify the heteroclinic type of phase turbulence in the experiment have failed so far. The reason is that the phase turbulence in which axial rolls become unstable to hexarolls which are quickly replaced again by axial rolls 180° degrees out of phase with the original ones occurs at Rayleigh numbers within 10% above the critical value. But this region is not accessible to the visualization technique employed in the present study because the amplitude of temperature variations is too small to induce a clearly visible color change in the liquid crystal sheets. Instead another form of phase turbulence has been observed in the experiment as shown in Fig. 7. This kind of

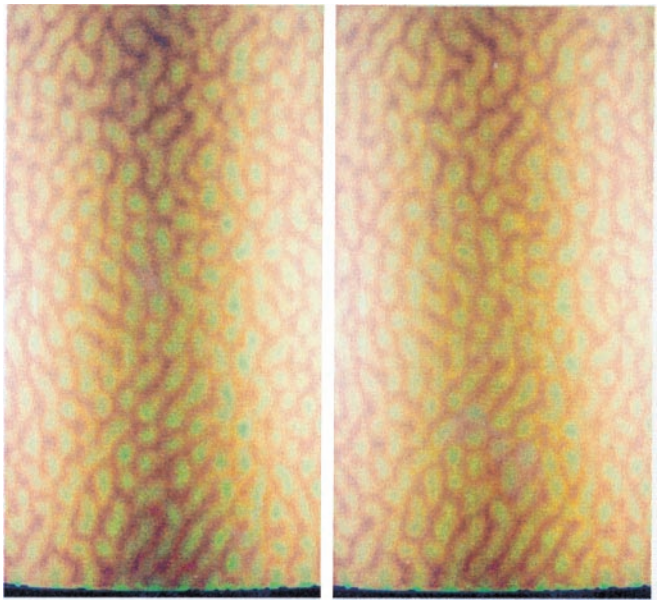

Fig. 7. Patterns of phase turbulent convection for $\tau = 11$, $R = 2{,}540$. The two photographs have been taken about 10 sec apart such that only small changes between left and right pictures can be noticed.

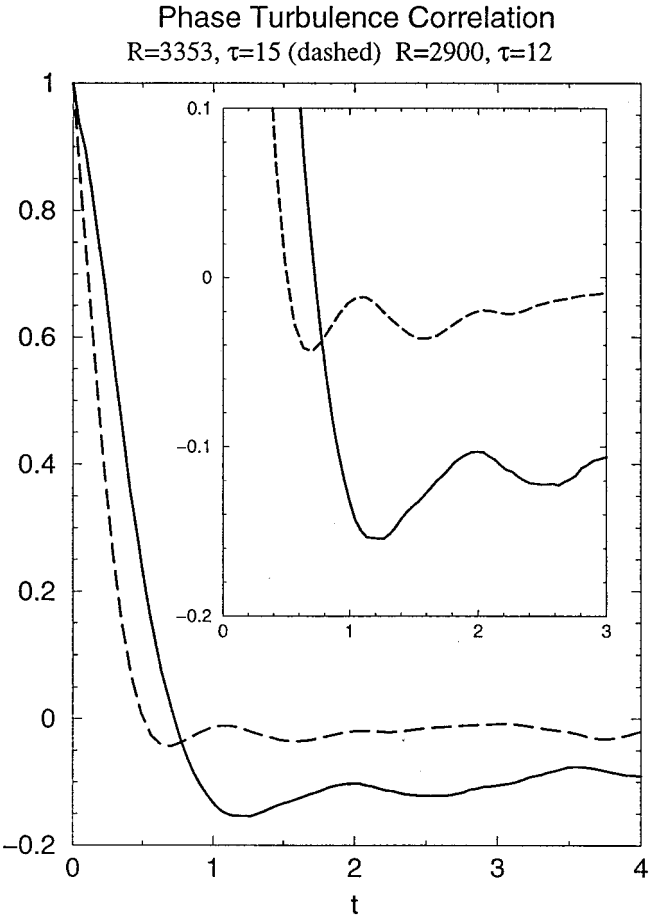

Fig. 8. Correlation function $C(t)$ as defined by **4** for phase turbulent convection patterns in the cases $\tau = 12$, $R = 2{,}900$ (solid lines) and $\tau = 15$, $R = 3{,}350$ (dashed lines). Insert provides enlargement around $C(t) \approx 0$.

phase turbulence appears to be connected with the phenomenon of knot convection rather than the phase turbulence originating from the hexaroll instability studied by Busse *et al.* (4). A detailed theoretical study of the phase turbulent convection as shown in Fig. 7 has not yet been done. But the origin of the phase turbulence from a cyclical process is evident in the correlation functions of the time dependent patterns. Two typical examples are shown in Fig. 8. In this figure the expression

$$C(t) = \sum_m K_m(t) \qquad [4]$$

has been plotted where the $K_m(t)$ are defined by

$$K_m(t) \equiv \sum_n a_n(t_m)a_n(t_m + t)[\sum_n (a_n(t_m))^2 \sum_n (a_n(t_m + t))^2]^{-1/2}.$$

Here the summation over n runs over all pixel value $a_n(t_m)$ of a charge-coupled device image of the convection pattern at the time t_m multiplied pixel values $a_n(t_m + t)$ at the same place n at the later time $t_m + t$. The time t varies in multiples of separation Δt of the equidistant times t_m at which pictures were taken. For the data of Fig. 8 $\Delta t = 5$ sec was used. Because the two data sets included about 250 pictures and times t up to 500 were considered the summation over m in 4 runs through about 150 pictures. More detailed studies of the correlation functions in the dependence on the parameters R and τ will be needed to determine the parameter dependence of the apparent oscillation period in Fig. 8. The period appears to decrease strongly with R until at values of the order of 5,000 a minimum in the correlation functions can no longer be discerned.

5. Concluding Remarks

The experiments reported in this paper have revealed some unusual patterns of centrifugally driven convection. Knot convection and hexaroll convection have been observed as predicted by the earlier theoretical analysis (3). But oblique rolls are also realized in the experiment for which detailed theoretical analyses are not yet available. The new system of high Prandtl number convection in the rotating cylindrical annulus offers new opportunities for observing transitions between different kinds of spontaneous dynamical patterns and for the study of the phenomenon of phase turbulence. Current research is aimed at a more comprehensive theoretical understanding of the observed phenomena. Future experiments will eventually be carried out in order to resolve questions arising from the mathematical analysis of the problem.

We wish to thank Mr. O. Brausch for his help in computing the correlation functions. The research reported in this paper has been supported through the Deutsche Forschungsgemeinschaft.

1. Busse, F. H. (1989) in *Mantle Convection*, ed. Peltier, W. (Gordon and Breach Publ., New York), pp. 23–95.
2. Busse, F. H., & Carrigan, C. R. (1974) *J. Fluid Mech.* **62,** 579–592.
3. Auer, M., Busse, F. H. & Clever, R. M. (1995) *J. Fluid Mech.* **301,** 371–382.
4. Busse, F. H., Brausch, O., Jaletzky, M. & Pesch, W. (2000) in *Intermittency in Turbulent Flows and other Dynamical Systems*, ed. Vassilicos, J. (Cambridge Univ. Press, Cambridge, U.K.), in press.
5. Busse, F. H. (1967) *J. Fluid Mech.* **30,** 625–649.
6. Busse, F. H. & Clever, R. M. (1979) *J. Fluid Mech.* **91,** 319–335.
7. Busse, F. H. & Clever, R. M. (1999) in *Pattern Formation in Continuous and Coupled Systems*, eds. Golubitsky, M., Luss, D. & Strogatz, S. H. (Springer, New York), pp. 25–32.